

System engineering the Space Infrared Interferometric Telescope (SPIRIT)

T. Tupper Hyde, David T. Leisawitz, David A. Di Pietro, and Stephen A. Rinehart
NASA Goddard Spaceflight Center (GSFC), 8800 Greenbelt Rd., Greenbelt, MD 20771

ABSTRACT

The Space Infrared Interferometric Telescope (SPIRIT) was designed to accomplish three scientific objectives: (1) learn how planetary systems form from protostellar disks and how they acquire their inhomogeneous chemical composition; (2) characterize the family of extrasolar planetary systems by imaging the structure in debris disks to understand how and where planets of different types form; and (3) learn how high-redshift galaxies formed and merged to form the present-day population of galaxies. SPIRIT will accomplish these objectives through infrared observations with a two aperture interferometric instrument. This paper gives an overview of SPIRIT design and operation, and how the three design cycle concept study was completed. The error budget for several key performance values allocates tolerances to all contributing factors, and a performance model of the spacecraft plus instrument system demonstrates meeting those allocations with margin.

Keywords: SPIRIT, Infrared/IR, Interferometry, Telescope, System Engineering, Error Budget

1 INTRODUCTION

The Space Infrared Interferometric Telescope (SPIRIT) will provide integral field spectroscopy throughout the wavelength range 25 – 400 μm with sub-arcsecond angular resolution and $\lambda/\Delta\lambda = 3000$ spectral resolution in a 1 arcminute instantaneous field of view. Many of the astronomical targets of interest will be resolved for the first time at far-IR wavelengths. SPIRIT's spatially resolved spectra will break model degeneracy and enable a new physical understanding of forming stars and planetary systems, mature planetary systems, and galaxies.

A single scientific instrument gives SPIRIT its powerful combination of spatial and spectroscopic measurement capabilities. SPIRIT is a Michelson stellar interferometer with a scanning optical delay line for Fourier transform spectroscopy and compensation of external optical path length differences. Following beam combination in the pupil plane, detector arrays multiplex the area coverage, expanding the field of view from the diffraction spot size of the individual light collecting telescopes to the desired arcminute scale. SPIRIT's two telescopes can be moved to sample many interferometric baselines, and therefore spatial structure on all of the angular scales necessary to produce high-quality far-IR images. The image resolution, 0.3 ($\lambda/100 \mu\text{m}$) arcsec, is determined by the maximum baseline length, 36 m. To attain superlative sensitivity, limited by astrophysical background photon noise, the SPIRIT optics are cooled to 4 K and sufficiently sensitive detectors will be used.

The results of a pre-Formulation Phase study of the SPIRIT mission concept are given in a series of papers, of which this paper is one. The scientific objectives, measurement requirements, and an overview of the design concept are described by Leisawitz et al. (2007).^[1] Wilson et al. (2007)^[2] describe the optics and stray light trades. Budinoff et al. (2007)^[3] describe the SPIRIT mechanical design and mechanisms and explain how the mechanical design will meet instrument stability, thermal and packaging requirements. DiPirro et al. (2007)^[4] present the thermal design concept, thermal modeling results, and the cooling power requirements, and they explain how cryocoolers will be used to meet these requirements. Benford et al. (2007)^[5] describe detector requirements, including NEP, pixel count and readout speed, and present the rationale for using small arrays of TES bolometers. Rinehart et al. (2007)^[6] update the status of our development of the wide-field imaging interferometry technique applicable to SPIRIT, and Martino et al. (2007)^[7] describe a model of the Wide-field Imaging Interferometry Testbed, a model which can be adapted to simulate interferometric data from SPIRIT. This paper covers the system engineering of SPIRIT: a walk-through of SPIRIT's design and operation, a re-cap of the three design cycle concept study, and an error budget and performance estimates for key interferometric performance metrics.

*Tupper.Hyde@nasa.gov; phone 301 286 5386; Applied Engineering and Technology Directorate, NASA GSFC.

2 SPIRIT DESIGN OVERVIEW

SPIRIT is a Michelson (pupil plane combining), double Fourier infrared interferometer which operates by collecting science light in two telescopes separated by a baseline. Figure 1 shows the functional layout of the SPIRIT instrument. Figure 2 shows the full observatory. The baseline is variable from 6 to 36 m by moving the telescopes on trolleys along a boom, symmetrically from the center. The light is compressed and steered into a combining instrument in the center. Here, the beam from each telescope is further compressed, collimated, and steered into a delay line with multiple passes and channel outputs and then combined with a beam from the other telescope. Following combination, the beam is focused onto a set of detector arrays. Shorter wavelength (2 micron) pickoffs from the science beams are interfered to create a zero path delay sensor and an angle sensor. A separate internal metrology laser interferometer measures the delay line stroke. Thermal barriers and cryocoolers allow for 4 K optics, 1 K final beam combining, and 50 mK ADR cooled focal planes. A “walk-through” of the instrument is now given by following the science light...

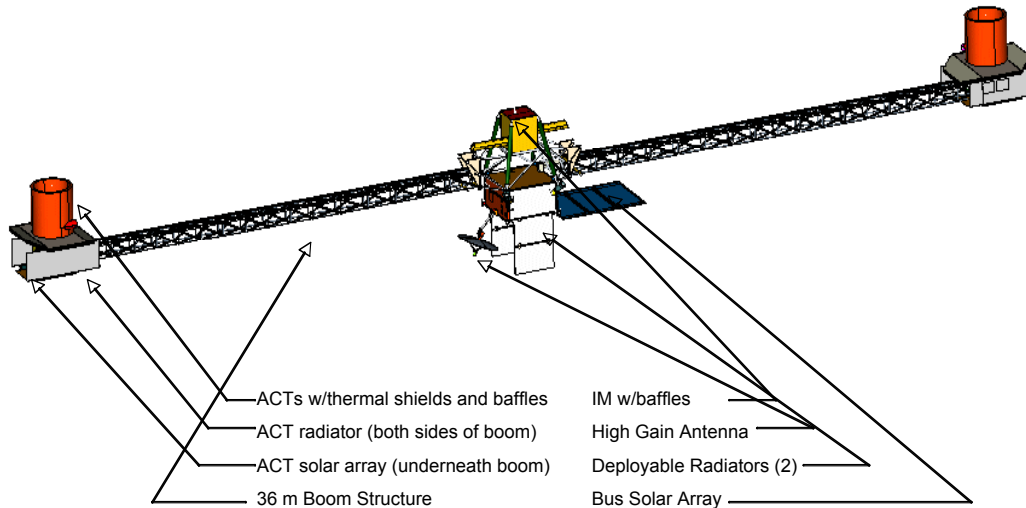


Figure 2: SPIRIT consists of a spacecraft bus supporting an instrument module (IM) and two array collector telescopes (ACTs) on deployable booms. Other deployables are solar array, high gain antenna, and two radiators.

2.1 Collector Telescope

There are two collector telescopes, on the two ends of the boom. Each collects, compresses, collimates, and steers the science light onto the central beam combiner. The primary telescope is an off axis parabola (OAP) 1.0 m in diameter. Making the primary larger allows better sensitivity or shorter integration times, but adds mass, cryo-cooler power, and makes packaging in the shroud more challenging. At the selected diameter, the optics are fixed; there are no deployments in the optical train. Smaller telescopes also widen the single telescope point spread function and reduce the number of array pixels required for a given field of view (FOV). The secondary mirror is an OAP on a six-axis mechanized mount (the secondary mirror pointing mechanism, SMPM) that corrects for alignment errors, focus, and periodic large pointing corrections. The third optic in the science light chain is the collector steering mirror (CSM), a flat mirror which folds the collimated beam and directs it to the central combiner with small stroke, but high bandwidth pointing correction. The beam is collimated after leaving the secondary making for a 10cm SM and CSM. The degree of beam compression is an important trade discussed in Wilson et al. (2007)^[2]. An optics bench provides the near zero CTE, structural connection for the three telescope optics.

The whole collector telescope sits in and on sunshields; details in DiPirro et al. (2007)^[4]. The remaining components are on the warm side. A trolley mechanism periodically adjusts the distance along the boom, thereby setting variable baselines. A collector telescope pointing mechanism provides rough (10 arcsec over 3 deg) pointing of the entire assembly to allow both left and right collector telescopes to boresight the same star on the sky. A bearing and distance sensor head works with similar units on the central combiner to give coarse relative bearing angles and distance measurements between the collector and central combiner. Finally, there are electronics on each collector unit: a solar array, mechanism drive electronics, and a wireless transceiver for data link back to the central combiner electronics.

2.2 Combiner Instrument

The combiner instrument sits in the center of SPIRIT and receives the science light from the left and right collector telescopes and interferometrically combines them creating multiple bands of output images. A series of shrouds keep the interior optics cold. A thermal baffle surrounds the incoming light port, thereby keeping thermal flux from warm parts of the collector from reaching the detector. The length and diameter of the thermal baffles, both on the combiner and collector, were a major thermal/structural system trade; see Wilson et al. (2007)^[2]. The incoming beams are compressed further to allow smaller optics in the delay line; again the degree of compression is an important trade covered in Wilson et al. (2007)^[2]. A shutter is placed in each leg and used in instrument alignment and calibration. By blocking the light from one arm, a single telescope imaging instrument is created from the other arm. A combiner beam steering mirror (CBSM) nulls the angle errors in the incoming beam. Having steering mirrors in both the collector and the combiner allow de-coupling of the integration and test of these two subsystems (see Wilson et al. (2007)^[2]), as well as allow for control of both beam pointing and beam overlap (discussed in this paper, section 4.2 and 4.3). A dichroic splits off the near infrared (2 micron) light for use in the two science metrology sensors; the zero path delay (ZPD) sensor keeps the interferometer on the central combined fringe, and the angle sensor (AS) measures the overall pointing of the two arms of the interferometer. Choosing the much shorter wavelength near infrared light was a trade in that it provides better angular and path length resolution but requires instrument wavefront error and pathlength stability to a fraction of that shorter wavelength for acceptable fringe visibility in the ZPD sensor.

The science light then enters a delay line with four output ports, one for each wavelength band channel. The shortest band (25-50 micron) makes just one pass through the delay length and exits through a wire grid beamsplitter. Successively longer bands (50-100, 100-200, and 200-400 micron) go through additional passes of delay. The physical stroke of the delay line needs to be just 6.15 cm to provide 86 cm of optical delay to the longest band output; resulting in a spectral resolution, R , of 3000 for the center (geometric mean) of that band. The shorter bands have higher R as shown in Figure 3. Details of the multi-pass, multi-output delay line optics and mechanism are given in Wilson et al. (2007)^[2] and Budinoff et al. (2007)^[3] respectively.

Each channel output beam then goes on to the Michelson beam combiners (beamsplitters) where they are interfered with the light from the other arm and pass into twin detectors with focusing optics and detector arrays. Using both outputs from the beam combination improves sensitivity and provides fault tolerance (with 3dB loss of sensitivity upon one detector failure). The detectors are housed in a 1 K shroud and cooled with ADRs to 50 mK. Total photometric efficiency (including optical throughput and detector efficiency) is greater than 18 percent. The detector pixel count is determined by the FOV and the point response of a single telescope at the diffraction limit. A separate metrology interferometer (the path length sensor) measures the differential pathlength between the two arms in the delay lines to 0.5 micron resolution. A laser in the warm side of the instrument feeds it by fiber. A thermal shield divides the cold side from the warm side components. The warm-side components of the cryo-cooler and ADR are below the shield. Two range and bearing metrology sensor heads are aimed at each of the collector telescope units. Instrument electronics include the interfaces for: focal planes, mechanisms, metrology, cryo-cooler, ADR, wireless transceivers to the collector telescopes, instrument command and data handling with 1553 interface to the spacecraft.

2.3 Spacecraft and orbit

SPIRIT will operate from a halo orbit about the Sun-Earth L2 point. This is an attractive location because it provides a stable, cold thermal environment and a relatively constant distance from the Earth for communication. The SPIRIT observatory is shown in Figure 2. The full observatory is 4497 kg (incl. 25% contingency). The spacecraft bus supports the combiner instrument module (IM) and the 36m deployable boom with the two collector telescopes. Thermal shields for the collector telescopes and the IM provide for a +/-20 deg field of regard (FOR) in two axes about the line to the

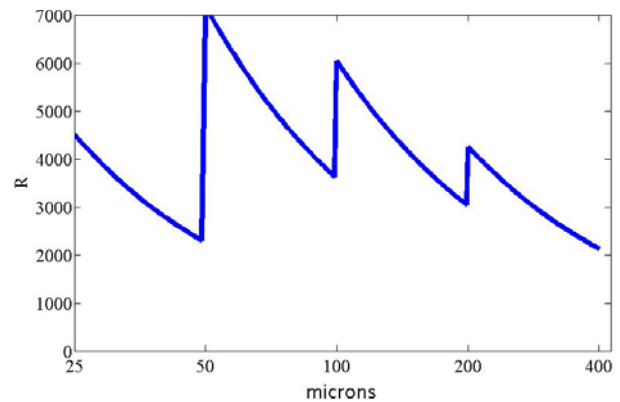


Figure 3: Achieved spectral resolution, R , as a function of wavelength for a delay line with 6.15 cm of physical stroke. The center (geometric mean) of the 200-400 micron band was set at 3000 after 7 passes of the delay line. Shorter wavelength bands make fewer passes: 1 for the 25-50 band, 3 for the 50-100 band, and 5 for the 100-200 band.

target. In SPIRIT's L2 halo orbit, this provides full target coverage around the ecliptic plane up to +/- 20 degrees ecliptic latitude. This FOR selection was a strong trade parameter in celestial coverage versus size of the thermal shields; at 20 deg the thermal shields do not need to be deployable. The spacecraft uses deployable booms, radiators, solar arrays, and high gain antenna to fit in the launch fairing.

The spacecraft bus has the typical subsystems and is similar to, but smaller than, the JWST spacecraft bus. It consists of a box structure approximately 1.5 m on a side with electronics and propellant tank mounted inside and deployables and thrusters mounted outside. The propulsion system is hydrazine monopropellant. The attitude control system (ACS) consists of six reaction wheels of 100 Nms each providing a slew rate of 1 deg/min and supports an average collection rotation rate of 0.63 rot/hr. Star trackers and gyros provide sensing for the coarse ACS control of 5 arcsec. This puts guide stars on the instrument's angle sensor for further accuracy. The communication system uses Ka-band for high data rate (100 Mbps) link and S-band for a contingency low data rate link. The electrical power system (EPS) consists of a solar array, battery, and power management electronics. The EPS supports the spacecraft systems and provides 1081 W for the IM (separate power systems on the collector telescopes have their own fixed solar arrays).

2.4 Operation

SPIRIT will be launched on a medium EELV with a 5 m fairing directly to its L2 transfer orbit. The spacecraft performs small correction and halo orbit insertion burns. SPIRIT will operate for 3 years with a 5-year goal (propellant for 5 years). Orbit station keeping maneuvers are performed infrequently (every few months). The primary driver for operations is science efficiency, that is, percent of total time spent integrating on detectors. Slewing to new targets, trolley positioning, alignments, calibration, and data downlink time must be minimized. Data downlinks occur every other day for two hours at 100 Mbps to DSN allowing 247 Gbit/day of science and housekeeping data 289 Gbit/day with encoding overhead). The degree of science data compression is addressed in Benford et al. (2007)^[5].

A typical observation begins by slewing to the new target, typically 10 degrees away in less than 2 hours. The spacecraft spins slowly about an axis towards target. Calibrations and alignments take a few minutes. The target is observed for 1/2 a revolution, and then the trolley moves to a new position (while the observatory continues to spin). Trolley spacing is dependent on desired U-V plane coverage but typically consists of 31 positions with baselines from 6 to 36 m. Downlinks interrupt science observations. During integration, the delay line is continuously stroked over the full range during the time the collecting telescopes have moved one half of a diameter tangentially due to spacecraft rotation. Images are read from the 8 focal planes (2 each of the 4 channels) which creates an on-board data set with baseline, rotation angle, and delay line position per image read. Frame read rates depend on stroke rate and channel. The frame rate is 573 Hz on the short wavelength channel typically. This results in a total uncompressed raw science data rate of 5.4 Mbps. The double Fourier interferometric data are post-processed on the ground to create an integral field spectroscopic data set with high spatial and spectral resolution. Total integration time depends on the desired sensitivity but typically is 24 hours of detector integration in 28.2 hour (29 hour with margin) total observation for 85 percent science efficiency and a 0.85 targets/day mission planning number.

3 SYSTEM ENGINEERING THE SPIRIT DESIGN CONCEPT

A SPIRIT pre-formulation study was conducted from August to December 2004 at NASA GSFC with science and engineering team partners. The objective was to develop one viable, not necessarily optimized, concept for accomplishing the SPIRIT mission. The goal was to maximize science return within given constraints, determine credible estimates for life cycle cost and development schedule, and identify program risks. This intense concept design phase built on previous instrument and mission design studies and was done for three point design cycles and trades.

3.1 A three design cycle concept study

The system engineering approach taken was to bracket the likely solution in the first two design cycles, then interpolate to determine technical capability (and resulting science return) corresponding to the cost constraints of the Origins Probe mission class. Figure 4 shows graphically the idea of a three design cycle concept study. The first (A) design cycle used the PI's notion of an ideal configuration as the starting point; an ambitious design. The second (B) design cycle evaluated the science "floor" mission; the point below which the science team believed science return would not justify the investment; an austere design. Trades were then introduced by each subsystem design lead and integrated by the instrument and mission system engineers to create a trade sensitivity and breakpoint matrix with overall system capabilities tied to costs and packaging feasibility. While the SPIRIT study engineers were conducting trades in

preparation for targeting the final (C) design cycle parameters, the scientists of the SPIRIT team were completing a design reference mission (DRM) with 15 “use cases” defined by individual science team champions. Established SPIRIT primary and secondary science goals were used to weight the science utility of the use cases. A set of measurement requirements was derived for each use case: field of view, field of regard, number of fields, wavelength range, spatial resolution, spectral resolution, and sensitivity. Evaluation of the DRM information allowed for informed targeting of the C design cycle parameter to get the most completion of the weighted DRM with a mission concept that would meet constraints. The PI and the full study team then met to define the targeted critical parameters for the final (C) design cycle. The results of the C design were those presented in the previous section. Table 1 lists critical parameters for the A, B, and C design cycles for side-by-side comparison.

3.2 Lessons learned

In analyzing the trades results from the A and B design cycles and pushing hard on the science driving use cases of the DRM, we found a few important things that were key elements of the C design: 1) high angular resolution is very attractive and therefore boom length was maximized given the available fairing volume, even at the expense of telescope diameter; 2) high spectral resolution was very attractive, even more so than high sensitivity, or FOV; 3) fixed (non-deployed) telescopes and sunshield elements save money, risk, and integration and test complexities; and 4) access to shorter wavelengths (down to 25 micron) was attractive, even at the expense of longer (over 400 micron) wavelengths. It cannot be understated how it really took the science team’s hard look at the science use cases of the DRM to drive out these realizations and target the C design cycle to get the most science in the available dollars (and in the medium EELV launcher class). An example of the benefits of the bracketing three design cycle concept study was that the 25-50 micron range was included at first in the A design just because it was a bounding point - there was no strong interest in it. In the later DRM analysis however, it became clear of that this range was attractive; the bracketing approach compelled people to think about the problem. As a result of seeing the problem from new and varied perspectives, the team discovered something unexpected and beneficial.

Table 1: Comparing key requirements and key configuration aspects of three design cycle concept study for SPIRIT. The C design used information learned from the A and B designs, trades and engineering breakpoints, along with science utility metrics derived from the science team’s design reference mission.

	A-Design (Ambitious)	B-Design (Austere)	C-Design (Final, Targetted)
Spectral Range	25-800 microns (5 octave bands)	50-400 microns (3 octave bands)	25-400 microns (4 octave bands)
Angular Resolution	.04 arcsec @ 25 microns (60 m boom length)	.21 arcsec @ 50 microns (24 m boom length)	.07 arcsec @ 25 microns (36 m boom length)
Spectral Resolution	R >= 1000 (860 mm ODL scan range, optical path/longest band)	R >= 100 (51 mm ODL scan range, optical path/longest band)	R >= 3000 (860 mm ODL scan range, optical path/longest band)
Field of View	2.5 arcmin (100 x 100 pixels)	1.0 arcmin (8 x 8 pixels)	1.0 arcmin (14 x 14 pixels)
Sensitivity	.35 to .70 mJ @ 1e6 sec (3 m collectors, 5e-19 W/rtHz detector noise)	3 to 6 mJ @ 1e6 sec (1 m collectors, 5e-19 W/rtHz detector noise)	3 to 6 mJ @ 1e6 sec (1 m collectors, 5e-19 W/rtHz detector noise)
Number of Observations	3600 (2/day for 5 years, 400 Hz frame rate, 574 Gbits stored, 50 Mbps downlink, 4hr/day, 10:1 comp.)	1800 (1/day for 5 years, 20 Hz frame rate, 6.3 Gbits stored, 1 Mbps downlink, 2hr/other day, 2:1 comp.)	900 (.85/day for 3 years, 793 Hz frame rate, 492 Gbits stored, 100 Mbps down, 2hr/other day, 2:1 comp.)
Sky Access	+/- 20 from anti-sun	+/- 20 from anti-sun	+/- 20 from anti-sun

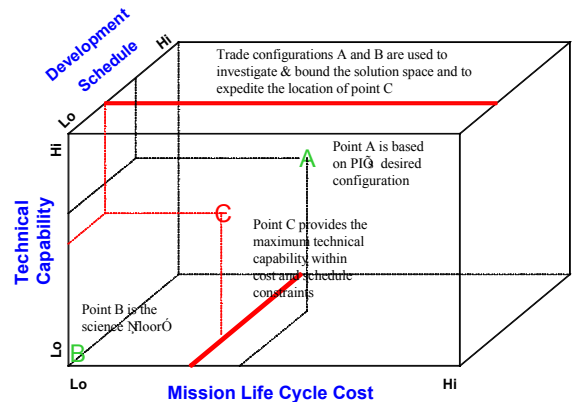


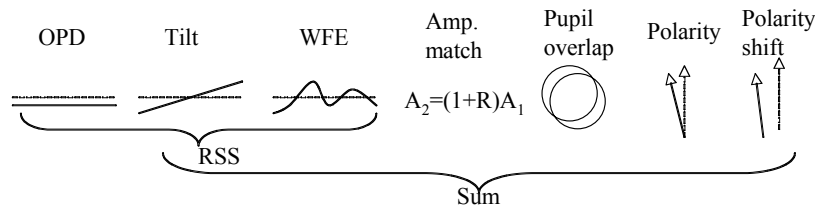
Figure 4: The system engineering approach to the SPIRIT conceptual design was to use three design cycles. The A design was done first based on the PI’s desired configuration. The B design was done second and met only the science “floor” requirements. This allowed informed so the final C design cycle could be targeted to yield the most science return given the constraints on mission life cycle cost and development schedule.

	(deployed sun shades)	(fixed sun shades)	(fixed sun shades)
Image Quality	Full u,v 95% visibility (1200 Nms momentum, 0.65 micron RMS wavefront match, 0.25 micron metrology)	Full u,v, 90% visibility (< 100 Nms momentum, 2.6 micron RMS wavefront match, 1.0 micron metrology)	Full u,v, 90% visibility (~300 Nms momentum, 1.3 micron RMS wavefront match, 0.5 micron metrology)
Mission Life (on station)	5 years	5 years	3 Years w/propellant for 5 yrs
Science Capability	Avg 1 target per 12 hrs	Avg 1 target per 24 hrs	Avg 1 target per 29 hrs
Science Field of View	2.5 arc min	1.0 arc min	1.0 arc min
Observing Rotation Rate	0.80 rev/hr (8.0 rev/obs)	0.45 rev/hr (9 rev/obs)	.63 rev/hr (15 rev/obs) avg.
Science Data Collect Rate	82Mb/s (derived)	57 kb/s (derived)	5.37 Mb/s (derived)
Optics Temperature	4 K	~>4 K (to 400 micron max)	4 K
Science Detector Temp	0.05 K	0.05 K	0.05 K
Phase B Start to Launch	67 mo. (incl. 6 mo. margin)	78 mo. (incl. 6 mo. margin)	72 mo. (incl. 10 mo margin)
Science Telescopes	2 Off-Axis	2 Off-Axis	2 Off-Axis
Telescope Diameter	3.0 m A-focal	1.0 m A-focal	1.0 m A-focal
Boresight Separation	(12-14 m) to 60 m Rigid Truss	6 m to 24 m Rigid Truss	6 m to 36 m Rigid Truss
Cryocooling	ACTDP coolers	ACTDP coolers	ACTDP (uprated) coolers
Sunshield Location	Above boom	Above boom	Above boom
Propulsion System	Hydrazine (monoprop.)	Hydrazine (monoprop.)	Hydrazine (monoprop.)
ACS Type /Accuracy	4 Rx Whl 75 Nms / 1.0 arcsec	4 Rx Whl 75 Nms / 1.0 arcsec	6 Rx Whl 100 Nms / 5.0 arcsec
Star Trackers	2 on Bus	2 on Boom	2 on Boom
Slew Rate (peak)	~1 degree per minute	~1 degree per minute	1.0 deg/minute
High Gain Antenna Type	Ka-Band – continuous 2 axis	X-Band – 2 axis gimbal	Ka Band – 2 axis gimbal
Ground Contacts	4.0 hr/day DSN, Ka Band	1.0 hr/day Com'l X-band	2.0 hour / 2 days DSN, Ka Band
Instrument Cold Mass	5346	2279	2828
Observ. Mass, Wet (kg)	6669	3591	4497
Instr Power, EOL (W)	820 for IM + 530 for 2 ACTs	555 for IM+ 568 for 2 ACTs	1081 for IM + 1036 for 2 ACTs
Fairing Diameter (m)	Delta IV 5m diam, 19m length	5m diam, (Atlas V Med)	5m diam, (Atlas V Med)

4 INTERFEROMETRIC ERROR BUDGET AND PERFORMANCE ESTIMATES

The SPIRIT interferometric error budgets are determined by two drivers: the need to achieve a visibility of > 0.90 at science wavelengths, and the need to achieve a visibility of > 0.25 at near infrared wavelengths for use with the metrology systems. Table 2 shows the visibility budget for SPIRIT at 2 and 25 microns.

Table 2: Sources of loss of visibility include mis-matches of pathlength, amplitude, pupil overlap, polarity and polarity shift. The driving terms in this interferometric error budget are the pathlength terms [piston optical path difference (OPD), tilt, and wavefront error(WFE)] for the 2 micron metrology light channel; each budgeted to be no more than 200 nm.



Term	dV formula	$\lambda=2$ micron		$\lambda=25$ micron	
		V>.25		V>.90	
OPD, rms	$(2\pi z/\lambda)^2$	0.200 um	0.3948	0.200 um	0.0025
Tilt, rms	$(2\pi(.177D\alpha)/\lambda)^2$	0.200 um	0.3948	0.200 um	0.0025
WFE, rms	$(2\pi\sigma/\lambda)^2$	0.200 um	0.3948	0.200 um	0.0025
Amp. match	$1-2/(R^{1/2}+R^{-1/2})$	30 %	0.0085	30 %	0.0085
Pupil overlap	$1-f_{\text{overlap}}$	98 %	0.0200	98 %	0.0200
Polarity	θ^2	6 deg	0.0110	6 deg	0.0110
Polarity shift	$(\theta/2)^2$	12 deg	0.0110	12 deg	0.0110
Result:		V=	0.255	V=	0.9419

These budgeted values lead to a 94 percent visibility at 25 microns wavelength and 26 percent visibility at 2 microns wavelength. Pupil area overlap contributes 2 percent loss of visibility. Amplitude, polarization, and polarization shift match all contribute about 1 percent visibility loss for each of these three terms. The beam wavefront matching terms (OPD due to piston, OPD due to tilt, and OPD due to differential WFE) contribute to negligible (0.8 percent) visibility loss at 25 microns about 69 percent visibility loss at 2 microns. Obviously it is the 2 micron metrology light case that drives fringe visibility requirements, so we will focus on that. Some of these sources of visibility loss listed above are mitigated through the use of controls. There are, however, several additional sources of visibility loss that cannot be compensated for by mechanisms. These include polarization, polarization shift, amplitude matching, and optical surface (WFE) errors.

4.1 Telescope Pointing: Bearing sensor and telescope pointing actuation

The pointing of the individual collectors is determined by two factors; the unvignetted field of view of the telescope and the angular range of motion of the collector steering mirror. The telescopes are accurately pointed by the spacecraft augmented with the range/bearing sensor to determine the position and orientation of the two telescopes relative to the spacecraft. The telescope mounts are then mechanized to move the entire telescope assembly. The field-of-view requirement is that the two telescopes should include an identical 1 arcmin FOV but have an unvignetted and unabated FOV of +/- 3 arcmin. The second requirement is due to the collector steering mirror; the telescopes must have absolute pointing to within the range of the collector steering mirror. The collector steering mirror range of motion will be at least 10 arcmin, which again does not provide a strong constraint on the telescope pointing. More importantly than this, the telescope pointing requirement leads to the required size of the collector steering mirror. The collector steering mirror (and the secondary) must be sized to accommodate the desired 1 arcminute FOV plus the additional FOV due to telescope mispointing. Ultimately, we have budgeted that the telescopes can be pointed to within 1 arcmin of the desired telescope FOV center.

The pointing of the telescope also needs to be stable between corrections, and any uncertainties in the pointing need to have amplitudes that are correctable through the use of the bearing sensor and the collector steering mirror. The thermal bending of the boom was shown by integrated analysis to be 0.3 mm static with the amplitude being reduced by an unknown factor for the rotating case. This equates to a sinusoidal variation of the telescope pointing of 3.4 arcsec at the revolution frequency. So the “good” FOV of the telescope must handle the 1 arcmin of initial pointing error as well as the 3.4 arcsec of thermal error that will come with SPIRIT rotation. The time varying thermal and spacecraft attitude pointing error will be removed downstream of the collector telescope. The requirements for this are rolled into the next section on controlling beam alignment.

Table 3: Telescope pointing error budget totals 1 arcmin (=60 arcsec); performance estimate is 13 arcsec.

Telescope pointing		Estimate	
1	Telescope pointing, percent of FOV		
60	Telescope pointing	arcsec	13 sum
20	Instrument Center (IM) pointing error	arcsec	4 calc
10	Contribution from RBS angle error	arcsec	10 calc
10	Contribution from telescope pointing mechanism	arcsec	1 calc
10	Contribution from motion not measured by RBS	arcsec	2 calc
10	Margin	arcsec	
5	Spacecraft pointing error (1 sigma)	arcsec	1 estimate from ST (spec is 5)
5	Spacecraft to IM alignment error (max physical)	arcsec	1 guess
4.85E-05	Allowed telescope pointing error (max physical)	rad	4.8E-06 calc
10.00	Allowed telescope pointing error (max physical)	arcsec	1 from MECH report
4.85E-05	Allowed RBS angle error (max physical)	rad	4.8E-05 calc
10	Allowed RBS angle error (max physical)	arcsec	10 from METR report
5	Allowed struct. deform. between RBS and telescope	arcsec	1 guess
5	Allowed calibration error of RBS to telescope	arcsec	1 guess

The flowdown of requirements through the telescope pointing error budget of 60 arcsec is shown above. The values are max and taken to be worst case (contributions are summed, not RSSed). The majority of the budget is given to the RBS angle sensor error and the rest to telescope pointing mechanism, RBS to telescope calibration error, RBS to telescope structural stability. There is 16 percent unallocated margin.

4.2 Beam Alignment: Bearing sensor and collector steering mirror actuation

Once the telescopes are accurately pointed, the collector steering mirror is used to accurately place the two beams on their respective combiner steering mirrors. Misalignment of the optical train by a certain percent of the beam will cause a mis-overlap of the combined beam in the pupil plane. A downstream pupil stop was considered to mitigate this, but this

is problematic as the physical pupil size changes as the trolley is moved in and out. The beam alignment is done in an open-loop fashion, making use of the bearing sensors. The bearing sensors, as designed, should accurately measure the position (translation) and pointing (angle) of the collector telescopes. This information is fed back to the collector steering mirrors, which make use of the information to steer the beam to the combiner steering mirrors. There is no feedback control to ensure that this pointing is accurate. The accuracy of the collector steering mirror, therefore, is required to at least as good as the accuracy of the bearing sensors, since we do not have any way of determining if fine corrections are necessary. The accuracy for these components is determined by the need to align the two beams on their respective combiner steering mirrors. We have assumed that this coalignment needs to be 2% of the beam diameter at the combiner steering mirror. This requirement is most stringent at the longest baseline. The collector steering mirror will update its position at roughly 2 Hz based upon the readings from the bearing sensor, in order to account for possible flexure in the boom due to thermal deformation (estimated by integrated thermal structural analysis to be 3.4 arcsec). Effects occurring faster than 2 Hz are beyond the scope of this mechanism (and, in fact, all our mechanisms) and should therefore be minimized in other ways.

Table 4: Beam alignment error budget totals 2 percent of beam area (= 3.05 mm beam walk at ZPD combiner); performance estimate is 2.56 mm.

Beam Alignment Budget			Estimate	
0.02	Mis-overlap ratio of area			
152.360	Size of beam at ZPD combiner	mm		
3.047198	Allowed beam walk (single axis) at combiner entrance	mm	2.55993	sum
1	Contribution from RBS translational error	mm	1	calc
1	Contribution from RBS angle error	mm	0.87266	calc
0.6	Contribution from motion not measured by RBS	mm	0.6	calc
0.1	Contribution from collector steering error	mm	0.08727	calc
0.347198	Margin			
18000	Effective distance from collector to combiner	mm		
5.56E-06	Allowed collector steering error (max physical)	rad	4.8E-06	calc
1.15	Allowed collector steering error (max physical)	arcsec	1	from MECH report
5.56E-05	Allowed RBS angle error (max physical)	rad	4.8E-05	calc
11.46	Allowed RBS angle error (max physical)	arcsec	10	from METR report
1	Allowed RBS translation error (max physical)	mm	1	from METR report
0.30	Allowed calibration error of RBS to optics train	mm	0.3	guess
0.30	Allowed struct. deform. between RBS and optics train	mm	0.3	guess

The flowdown of requirements through the beam alignment error budget of 3.05 mm is shown above. The values are max and taken to be worst case (contributions are summed, not RSSed). The majority of the budget is given equally to four errors. Max allowed requirements are: RBS angle sensor error (11 arcsec), RBS translation error (1.0 mm), collector steering mirror error (1.15 arcsec), RBS to optics train calibration error (.30 mm), RBS to optics train structural stability (.30 mm). There is 11 percent unallocated margin.

4.3 Tilt: Angle sensor and combiner steering mirror actuation

Once the beams from the two arms are aligned to a small fraction of a beam diameter at the combiner steering mirror, there remains the possibility that the two beams, as they enter the combiner, are coming in at an angle. This leads to a relative wavefront tilt between the two beams, and a subsequent loss in visibility related through the Jinc function. Furthermore, this angular tilt will lead to a small offset in the positions of the two beams as they impinge upon the detectors, leading to further loss in visibility. In order to minimize this effect, we require that the angle sensor accurately measure the relative wavefront tilt between the two beams and feed this back to the combiner steering mirrors which will remove the tilt. As with the collector steering mirror, the combiner steering mirrors will be updated at 2 Hz based upon the readings from the angle sensor. This, unlike the collector steering mirror and the bearing sensor, is a closed-loop process, as the angle sensor will provide effectively immediate feedback on the relative position of the combiner steering mirror. This image motion compensation (IMC) loop will have a 0.2 Hz bandwidth (unity gain frequency) with a 2 Hz sample rate (10 x rule of thumb for acceptable loop phase loss).

The flowdown of requirements through the differential tilt error budget of 0.23 arcsec (1 sigma, on the sky) is shown above. The values are taken to be 1 sigma over the integration time of the ZPD sensor (contributions RSSed). The budget is divided equally between the sensor noise, actuation noise, and unrejected disturbances. There is also a small contribution from the non-common path errors associated with the sensor (the angle sensor) not being co-located with the sensitive instrument (the ZPD interferometer). There is 11 percent unallocated margin.

Table 5: Tilt error budget totals 0.23 arcsec (on-sky) at ZPD sensor; performance estimate is 0.13 arcsec.

Tilt (Pointing), rms on sky Budget			Estimate
0.23	Dif Tilt rms at ZPD sensor over integration time	arcsec	0.12672 RSS
0.10	Contribution from angle sensor noise	arcsec	0.1 calc
0.10	Contribution from actuation noise	arcsec	0.06325 calc
0.05	Contributions not measured at angle sensor	arcsec	0.04243 calc
0.15	Contribution from unrejected disturbances	arcsec	0.01608 calc
0.022	Margin	arcsec	
0.50	integration time of ZPD sensor	sec	
2.00	Angle sensor readout rate	Hz	
0.50	integration time of angle sensor	sec	
0.20	Bandwidth of image motion compensation loop	Hz	
0.10	Allowed angle sensor NEA (1 sigma) in band	arcsec	0.1 from MET report
1.06	Allowed combiner steering mirror noise (1 sigma, physical), out of band	arcsec	0.3 from MECH report
0.35	Allowed collector steering mirror noise (1 sigma, physical), out of band	arcsec	0.3 from MECH report
0.03	Allowed calibration error of ZPD tilt to AS	arcsec	0.03 guess
0.03	Allowed stability of ZPD tilt to AS	arcsec	0.03 guess
0.14	Allowed unrejected errors at .02 Hz (ACS)	arcsec	0.0045 calc
0.02	Allowed unrejected errors at 1/rev (thermal)	arcsec	0.01543 calc
0.06	Allowed other unrejected tilt disturbances (jitter)	arcsec	0.0001 calc
20.00	Rejection factor at .02 Hz		
2.70	Allowed open loop errors at .02 Hz (ACS)	arcsec	0.09 from ST and Gyro KF
0.00077	1/rev frequency	Hz	
13365.30	Rejection factor at 1/rev freq		
200.48	Allowed open loop errors at 1/rev freq (thermal)	arcsec	3.43775 calc
1049.71	Allowed open loop errors at 1/rev freq (thermal)	mm	0.3 FROM STOP report
63.64	Allowed pointing jitter (above control bandwidth)	mas	0.1 from RWA imbalance

From this allocation, 1 sigma allowed requirements are: angle sensor noise (.10 arcsec), and unrejected (out of band) collector steering mirror noise (1.06 arcsec, physical = 0.07 arcsec on sky) and collector steering mirror noise (0.35 arcsec physical = 0.07 arcsec on sky). These are 1 sigma noise allocations over the 2 Hz bandwidth of the ZPD sensor. They may be due to quantization (divide by square root of 12) or amplifier noise. Further, the allowed calibration and stability (between calibrations) requirements for alignment of the angle sensor null point to the true ZPD zero tilt condition are 0.03 arcsec each. Finally the unrejected tilt disturbances are allocated to three categories. Those disturbances at .02 Hz (ACS and ODL imbalance induced) are rejected by the image motion compensation by a factor of 20 and can therefore be up to 2.7 arcsec open loop (spacecraft ACS is specified at 0.3 arcsec, 1 sigma and is predicted to do 0.09 arcsec, 1 sigma). Those disturbances at the once per SPIRIT revolution (thousands of seconds) are rejected by over 13,000 and can therefore be up to 200 arcsec (covers the 3.4 arcsec predicted thermal pointing motion at 1/rev). Finally, tilt disturbances at frequencies higher than the image motion compensation bandwidth of 0.2 Hz are given a total allocation of 63 mas (structural damping of 0.5 percent and well balanced RWAs allow the vehicle to meet this with significant margin, prediction is 0.1 mas due to RWA imbalance).

4.4 OPD: ZPD sensor and pathlength compensation

Once the beams are aligned and the wavefronts parallelized, there may remain a piston error difference between the two arms. This error is mitigated through use of the ZPD sensor and the pathlength compensator. The ZPD sensor makes use of a NIR guide star in the FOV of the instrument. The fringe pattern from this star is scanned to find the zero path difference (ZPD) point, and is then shifted to place the first zero-crossing of the fringe pattern in delay line space. Using the position of this zero-crossing, the pathlength compensation mechanism is used to adjust the total pathlength difference of the two arms of the interferometer (including the delay line) to 1/2 of the optical delay distance (i.e. so that the ZPD for the center of the FOV is at the center of the delay line range of travel). Then, as the delay line scans through the fringe pattern, the ZPD sensor monitors the zero-crossing, adjusting the path length compensator to keep the total path length of the two arms (prior to the ZPD sensor – i.e. prior to the delay line) constant. The sensor and mechanism together keep the total optical delay shift to less than a fraction of a wave of science light. The control must also stabilize the metrology (near IR) light on the ZPD sensor to a fraction of its wavelength over the integration time of the ZPD detector readout (0.5 sec) in order maintain visibility on the ZPD sensor fringe. The overall situation is actually a bit more stringent than this, as we require that the total piston error be small, and the total piston error consists of both errors prior to the delay line, and errors within the delay line itself. The latter are discussed in a later section.

The flowdown of requirements through the OPD error budget for the ZPD sensor of 0.20 micron (1 sigma) is shown above. The values are taken to be 1 sigma over the integration time of the ZPD sensor (contributions RSSed). The

budget is divided equally between the sensor noise, actuation noise, and unrejected disturbances. There is 10 percent unallocated margin.

Table 6: OPD error budget totals 200 nm; performance estimate is 143 nm.

OPD Budget			Estimate	
0.20	OPD rms at ZPD sensor over integration time	micron	0.14334	RSS
0.10	Contribution from ZPD sensor noise	micron	0.1	calc
0.10	Contribution from actuation noise	micron	0.1	calc
0.11	Contribution from unrejected disturbances	micron	0.02336	calc
0.021	Margin	micron		
2.00	ZPD readout rate	Hz		
0.50	integration time of ZPD sensor	sec		
0.20	Bandwidth of image motion compensation loop	Hz		
0.10	Allowed ZPD sensor NEA (1 sigma) in band	micron	0.1	from METR report
0.05	Allowed pathlength compensation noise (1 sigma, physical), out of band	micron	0.05	from MECH report, 1 sigma
0.09	Allowed unrejected errors at .02 Hz (ACS)	micron	0.00785	calc
0.07	Allowed other unrejected errors (jitter + negligible thermal)	micron	0.022	calc
2000.00	Rejection factor at .02 Hz (include int time factor)			
176.00	Allowed open loop errors at .02 Hz (ACS)	micron	15.708	calc
4.89E-06	Allowed open loop ACS pointing at .02 Hz	rad	4.4E-07	calc
1.01	Allowed open loop ACS pointing at .02 Hz	arcsec	0.09	from ST and Gyro KF (0.3 spec)
0.07	Allowed OPD jitter (above control bandwidth)	micron	0.022	from RWA imbalance

From this allocation, 1 sigma allowed requirements are: ZPD sensor noise (.10 micron), and unrejected (out of band) pathlength compensation noise (0.05 micron physical = 0.10 micron optical). The pathlength compensation mechanism noise is 1 sigma over the 2 Hz bandwidth of the ZPD sensor. It could be due to quantization (divide by square root of 12) or amplifier noise. Finally the unrejected OPD disturbances are allocated to two categories. Those disturbances at 0.02 Hz (ACS and ODL imbalance induced) are rejected by the image motion compensation by a factor of 20 (with another factor of 10 to account for the ratio of motion frequency to integration frequency) and can therefore be up to 176 micron open loop. This is equivalent to 1.01 arcsec over the 36 meter baseline (ACS is speced at 0.3 arcsec, 1 sigma and is predicted to do 0.09 arcsec, 1 sigma). And tilt disturbances at frequencies higher than the image motion compensation bandwidth of 0.2 Hz are given a total allocation of 0.07 microns (structural damping of 0.5 percent and well balanced RWAs allow the vehicle to meet this with significant margin, prediction is 0.02 microns OPD from wheel imbalance). Those disturbances at the once per SPIRIT revolution (thousands of seconds) are rejected by such as huge amount as to be negligible and are not included in the budget.

As mentioned above, piston error in the system consists of both piston error outside of the combiner (pre-delay line) and within the delay line itself (due to vibration, uneven motion, etc.). The latter should be a small effect, and as such, rather than having to control the delay line motion to better the same level of accuracy as the pathlength compensation mechanism, we need merely to have knowledge of the pathlength within the delay line to a small fraction of a fringe. For this purpose, knowledge of this path length to better than a small fraction of a fringe should be sufficient, say 0.5 microns. This should be easily achievable with laser metrology systems. It is also critical to calibrate any non-common path OPD between the ZPD sensor and each science detector. This is easily achieved by observing a bright point source on axis in all science detectors and the ZPD sensor simultaneously. The stability of that non-common path calibration should be quite stable (much better than the required 0.5 micron) due to the cold and very stable instrument module optics bench structure.

4.5 WFE (optical surface errors), amplitude matching, polarization, and polarization shift

A single aperture telescope has a non-ideal point spread function due to optical surface errors. An interferometer is more sensitive to optical surface errors because they cause the wavefront to have phase variations. These phase variations are the equivalent to local piston errors that do not match between one arm and the other, and therefore lead to a loss of fringe visibility. In general, for a given optical surface, the visibility loss due to surface roughness is given by $1 - e^{-(2\pi\sigma/\lambda)^2}$, where σ is the RMS of the difference in wavefront error (WFE) between the arms. This is approximately a loss of $(2\pi\sigma/\lambda)^2$ for small σ . This total budgeted WFE from the surfaces is 200 nm RMS. Further allocation to elements of the optical train is given in Wilson et al. (2007)^[2]. Remember that it is the differential WFE between the arms that matters; WFE from aberrations that are part of the design are identical in both arms and therefore not part of this budget (but are part of the Strehl and encircled energy calculations).

Amplitude matching (30 percent), polarization (6 degrees), and polarization shift (12 degrees) budgets are met easily; though attention to the design is necessary to make sure both arms have balanced number and rotation of reflections.

5 SUMMARY

Interferometric performance error budgets were flowed down from visibility requirements and allocated to subsystems (optics, sensors, controls, mechanisms, and structures). Performance estimates were then rolled back up based on the actual component performance reported in subsystem design documents. Table 7 gives a summary of visibility loss contributions. For science light at 25 microns, a 98 percent visibility is the performance estimated against a 90 percent requirement. For the more stringent near infrared metrology light at 2 microns, a 47 percent is the performance estimated against a 25 percent requirement for the visibility at the fringes on the ZPD sensor.

Table 7: Top-down error budget and bottom's up performance estimate for the 25 and 2 micron visibility.

Budget	Science Light (25 micron)	Estimate	Budget	ZPD Sensor (2 micron)	Estimate
0.0025	dV from OPD, rms	0.0013	0.326	dV from OPD, rms	0.184
0.0025	dV from Tilt, rms	0.0007	0.326	dV from Tilt, rms	0.110
0.0025	dV from WFE, rms	0.0025	0.326	dV from WFE, rms	0.326
0.008	dV from Total WFE (OPD, Tilt, and WFE)	0.005	0.694	dV from Total WFE (OPD, Tilt, and WFE)	0.511
0.009	dV from Amp. match	0.000	0.009	dV from Amp. match	0.000
0.020	dV from Pupil area overlap	0.017	0.020	dV from Pupil area overlap	0.017
0.011	dV from Polarity	0.001	0.011	dV from Polarity	0.001
0.011	dV from Polarity shift	0.001	0.011	dV from Polarity shift	0.001
0.058	Total dV	0.024	0.745	Total dV	0.530
0.942	Total uncalibrated visibility (Science), budget	0.98	0.255	Total uncalibrated visibility (ZPD), budget	0.47

This paper showed the basic design and operations for the SPIRIT concept. The three design cycle approach for conceptual design was explained. The science team's design reference mission was used to guide the design process through requirement specifications and performance appraisals.

The SPIRIT study team accomplished the goal, which was to demonstrate the scientific promise and technical viability of a space-based far-IR/ submillimeter spatial and spectral interferometer as a candidate Origins Probe mission. The IR community recommended SPIRIT in its "Community Plan," and the mission is well aligned with NASA programmatic and science objectives.

REFERENCES

1. Leisawitz, D., Baker, C., Barger, A., Benford, D., Blain, A., Boyle, R., Broderick, R., Budinoff, J., Carpenter, J., Caverly, R., Chen, P., Cooley, S., Cottingham, C., Croke, J., DiPietro, D., DiPirro, M., Femiano, M., Ferrer, A., Fischer, J., Gardner, J.P., Hallock, L., Harris, K., Hartman, K., Harwit, M., Hillenbrand, L., Hyde, T., Jones, A., Kellogg, J., Kogut, A., Kuchner, M., Lawson, W., Lecha, J., Lecha, M., Mainzer, A., Mannion, J., Martino, A., Mason, P., Mather, J.C., McDonald, G., Mills, R., Mundy, L., Ollendorf, S., Pellicciotti, J., Quinn, D., Rhee, K., Rinehart, S.A., Sauerwine, T., Silverberg, R.F., Smith, T., Stacey, G., Stahl, H.P., Staguhn, J., Tompkins, S., Tveekrem, J., Wall, S., and Wilson, M., The Space Infrared Interferometric Telescope (SPIRIT): High-resolution imaging and spectroscopy in the far-infrared, *J. Adv. Sp. Res.*, in press (2007), doi:10.1016/j.asr.2007.05.081
2. Wilson, M.E., Leisawitz, D.T., Martino, A.J., Rinehart, S.A., Croke, J.A., Tveekrem, J.L., Budinoff, J.G., Quijada, M.A., and Hyde, T.T., The Space Infrared Interferometric Telescope (SPIRIT): Optical system design considerations, *Proc. SPIE 6687*, this volume (2007).
3. Budinoff, J.G., Leisawitz, D.T., Rinehart, S.A., DiPirro, M.J., Jones, D.L., Hyde, T.T., and Taylor, B., Mechanical design of the Space Infrared Interferometric Telescope (SPIRIT), *Proc. SPIE 6687*, this volume (2007).
4. DiPirro, M.J., Cottingham, C., Boyle, R., Ollendorf, S., and Leisawitz, D.T., The SPIRIT thermal system, *Proc. SPIE 6687*, this volume (2007).
5. Benford, D.J., Rinehart, S.A., Hyde, T.T., and Leisawitz, D.T., Cryogenic far-infrared detectors for the Space Infrared Interferometric Telescope (SPIRIT), *Proc. SPIE 6687*, this volume (2007).
6. Rinehart, S.A., Armstrong, J.T., Frey, B.J., Jung, J., Kirk, J., Leisawitz, D.T., Leviton, D.B., Lyon, R.G., Martino, A.J., Mundy, L.G., Pauls, T.A., and Schurr, S., Wide-field imaging interferometry: An enabling technique for high angular resolution astronomy, *Proc. SPIE 6687*, this volume (2007).
7. Martino, A.J., Leisawitz, D.T., Thompson, A.K., Rinehart, S.A., and Frey, B.J., An optical model of the Wide-field Imaging Interferometry Testbed, *Proc. SPIE 6687*, this volume (2007)